a

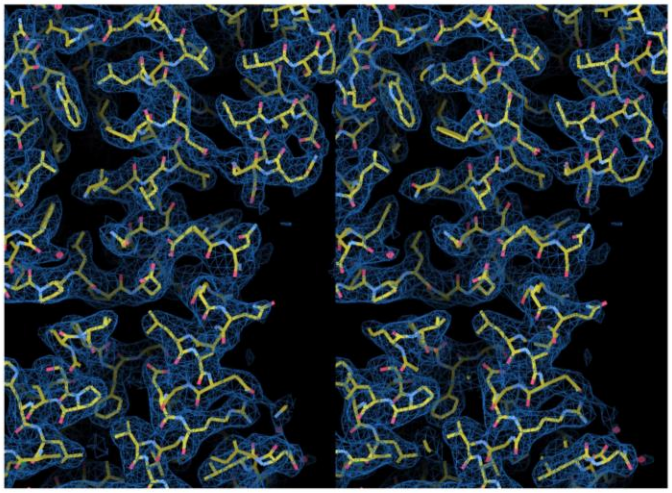

b

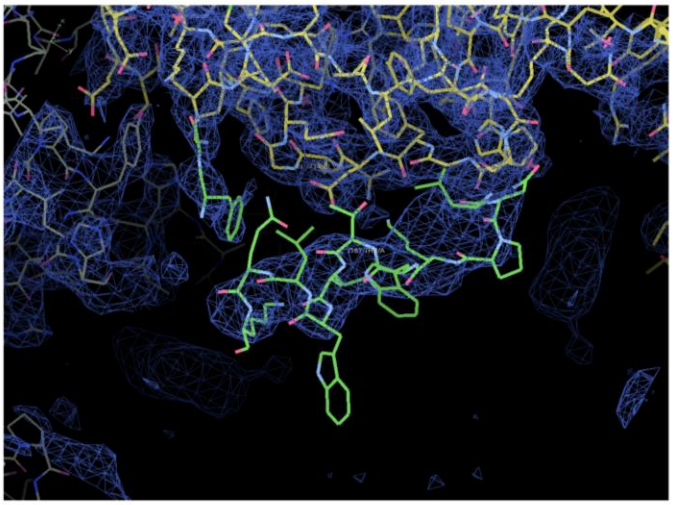

Supplementary Figure 1. Crystallography of PI4KIIα with ADP bound. a, A stereo image of overall 2Fo-Fc electron density map of PI4KIIα contoured at 1.0 σ. **b**, 2FoFc electron density map (1.0 σ) around the palmitoylation insertion, colored in green.

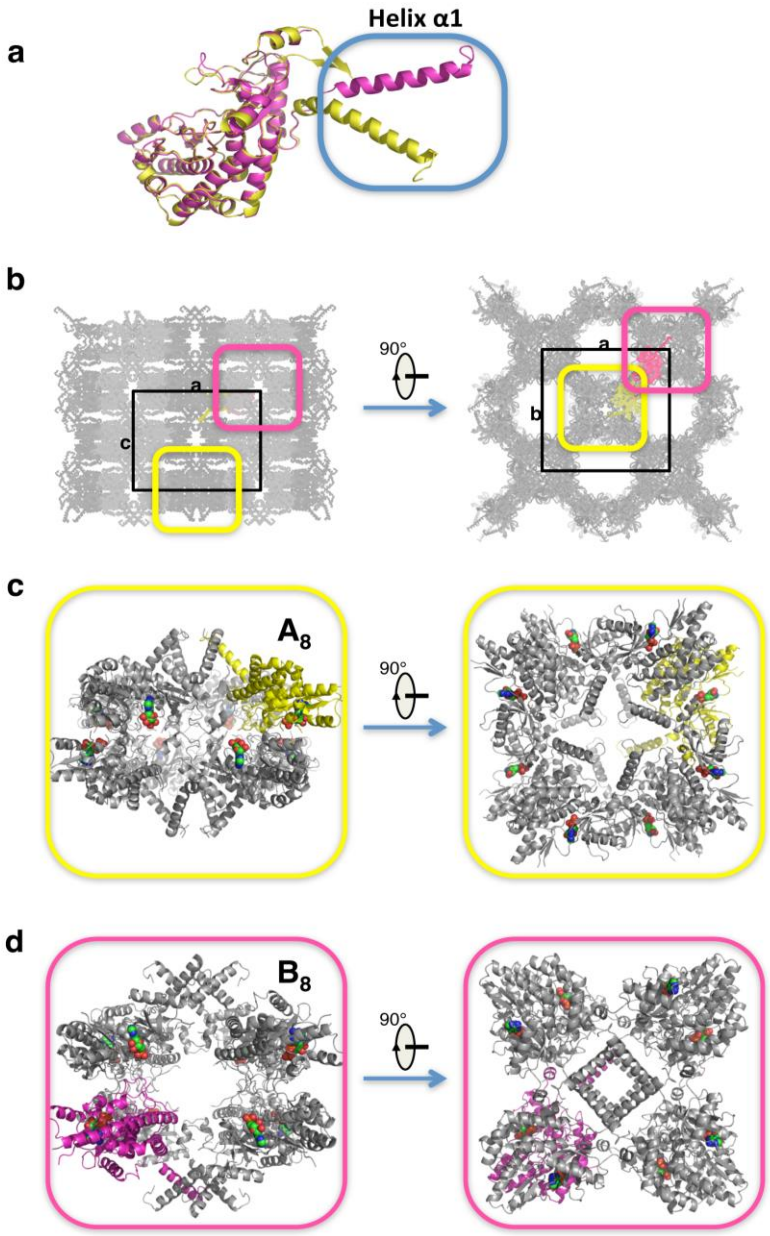

Supplementary Figure 2. Analysis of the crystal packing of PI4KIIα. a, Superposition of the two PI4KIIα molecules (A, yellow; B, pink) in one asymmetric unit. The significantly different conformations at the P-loop region and N-terminal helix α1 are indicated and labeled. **b,** Overall crystal packing of PI4KIIα viewed along the **b** axis (left) and **c** axis (right). The unit cell is depicted and labeled. The two molecules of PI4KIIα in one asymmetric unit are colored in yellow, molecule A, and pink, molecule B. Octamers (A_8 and B_8) formed by each type of molecule are

indicated by respective rectangles. **c** and **d**, Overall structures of the octamers A_8 and B_8 are viewed from along (left) and perpendicular to (right) the membrane binding surface of PI4KIIα. The bound ADP in each molecule is shown as a colored sphere. Color schemes for the rectangles are the same as in **b**.

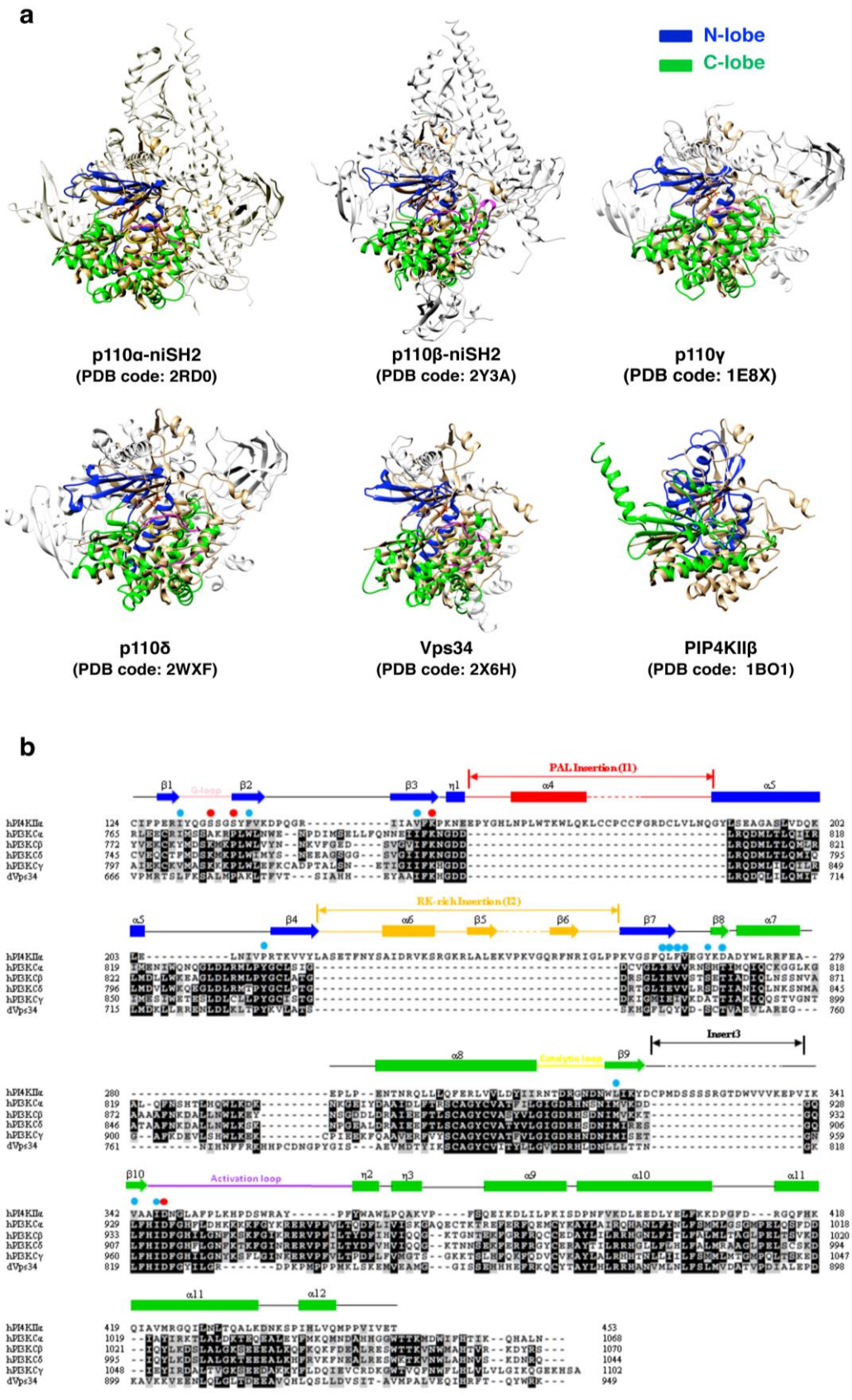
a
N-lobe
C-lobe
p110α-niSH2
(PDB code: 2RD0)
p110β-niSH2
(PDB code: 2Y3A)
p110γ
(PDB code: 1E8X)
p110δ
(PDB code: 2WXF)
Vps34
(PDB code: 2X6H)
PIP4KIIβ
(PDB code: 1BO1)
b
PAL Insertion (I1)
RK-rich Insertion (I2)
Insert3
Catalytic loop
Activation loop
hPI4KIIα
hPI3KCα
hPI3KCβ
hPI3KCδ
hPI3KCγ
dVps34

Supplementary Figure 3. Comparisons of the structures of PI4Ks and PI3Ks. **a,** Known crystal structures of class I PI3K (p110 α, β, γ and δ), class III PI3K (vps34) and PIP4KII β are shown as cartoon diagrams with the structure of PI4KIIα catalytic domain (colored in golden) superimposed, respectively. The views take the same angle as the crystal structure of PI4KIIα in **Fig. 1c**. The N- and C-lobes of the catalytic domain are colored in blue and green, respectively. The catalytic loop and activation loop (if present) are colored in purple and red, respectively. The corresponding PDB code is shown below each structure. **b,** Structure-based sequence alignment of the catalytic domains of PI4KIIα and PI3Ks**.** Structural superposition and the subsequent structure-based sequence alignment were performed using UCSF Chimera [1]. Secondary structures of PI4KIIα are shown and labeled above the sequences, with blue for the N-lobe and green for the C-lobe; dashed lines represent untraced regions of the PI4KIIα structure. Identical residues in the alignment are colored in black and similar residues in grey. Residues that contribute to nucleotide binding in PI4KIIα are marked as solid circles with residues interacting with the phosphate moiety in red(●) and residues interacting with adenosinein cyan(●). GenBank accession numbers for the amino acid sequences of these proteins are Q9BTU6 for hPI4KIIα, P42336 for hPI3Kα (p110α), P42338 for hPI3Kβ (p110β), O00329 for hPI3Kδ (p110δ), P48736 for hPI3Kγ (p110γ) and Q9W1M7 for dVps34. The figure was prepared using Boxshade3.21 (http://www.ch.embnet.org/software/BOX_form.html).

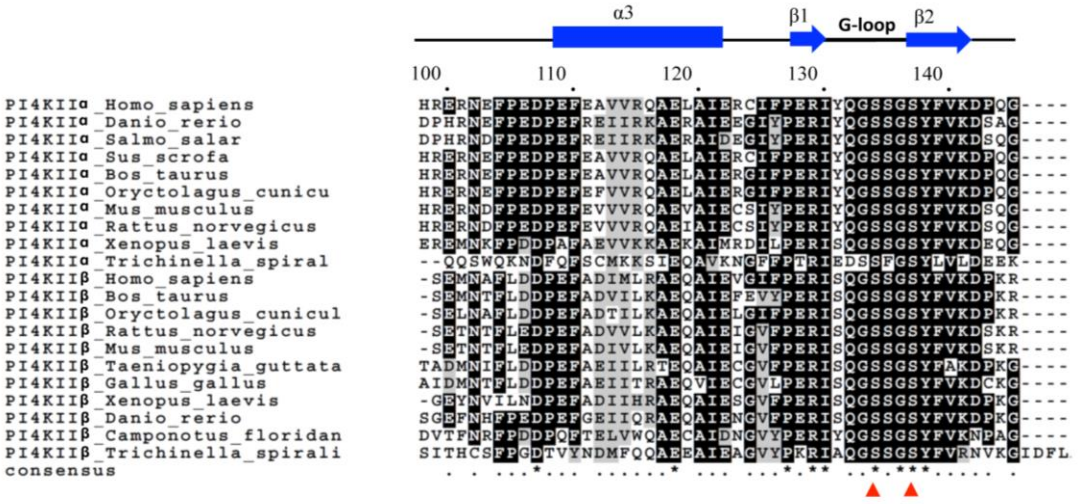

Supplementary Figure 4. Sequence alignment of PI4KIIs around the G-loop region. Ser134 and Ser137 residues are indicated with red triangles. The GenBank accession numbers of the PI4KIIα sequences from different species are NP_060895 for *Homo sapiens*, NP_998523 for *Daniorerio*, ACN11482 for *Salmosalar*, XP_001929069 for *Susscrofa*, NP_001093786 for *Bos Taurus*, XP_002718643 for *Oryctolaguscuniculus*, NP_663476 for *Musmusculus*, NP_446187 for *Rattusnorvegicus*, NP_001121279 for *Xenopuslaevis* and XP_003366872 for *Trichinellaspiralis*. The GenBank accession numbers of the PI4KII β sequences from different species are NP_060793 for *Homo sapiens*, NP_001095534 for *Bos Taurus*, XP_002709306 for *Oryctolaguscuniculus*, NP_001005883 for *Rattusnorvegicus*, NP_080227 for *Musmusculus*, XP_002191179 for *Taeniopygiaguttata*, NP_001026328 for *Gallus gallus*, NP_001087050 for *Xenopuslaevis*, NP_001038950 for *Daniorerio*, EFN64759 for *Camponotusfloridanus* and XP_003378208 for *Trichinellaspiralis*. The alignment was performed using ClustalW and the figure was prepared with Boxshade3.21 (http://www.ch.embnet.org/software/BOX_form.html).

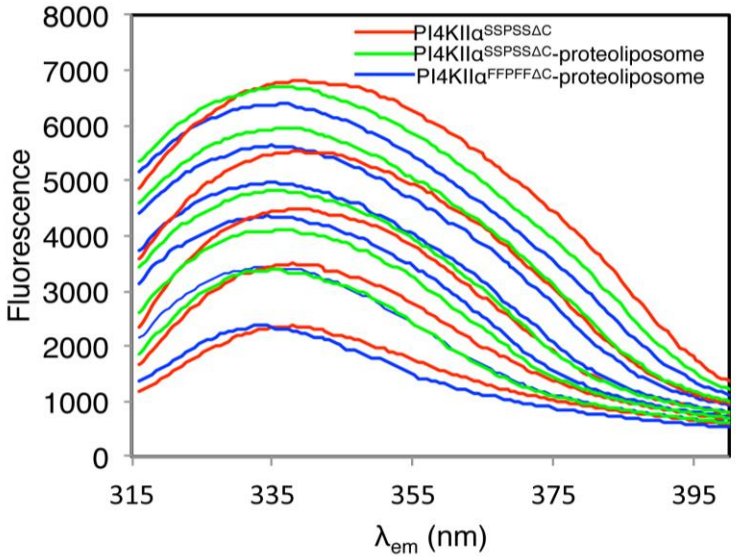

Supplementary Figure 5. Blue shifts in the internal fluorescence of Trp residues validates the membrane binding surface of PI4KIIα. In addition to the untraced Trp332 on insertion I2 and three non-exposed residues, Trp273, Trp314 and Trp366, the remaining four Trp residues (Trp359, Trp368, Trp166, Trp169) are exposed at the putative membrane-binding surface of PI4KIIα. Internal tryptophan emission fluorescences of PI4KIIα variants (PI4KIIα$^{SSPSS\Delta C}$ and PI4KIIα$^{FFPFF\Delta C}$), which were in solution or reconstituted into liposomes, were measured at different protein concentrations, using the excitation wavelength at 295 nm.

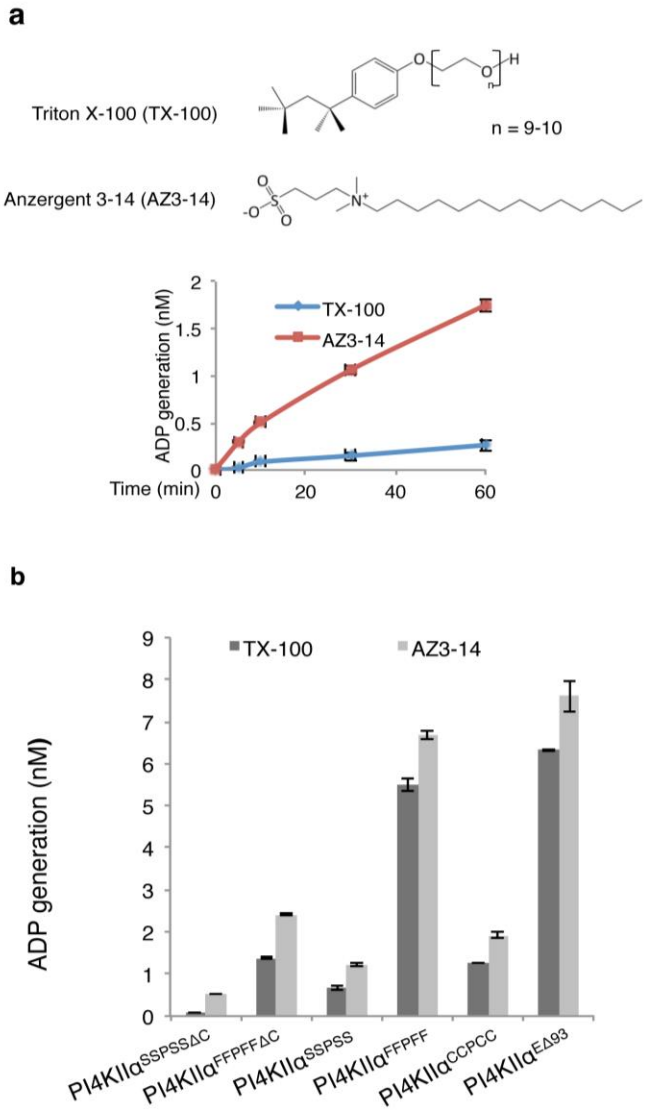

Supplementary Figure 6. Kinase activity of PI4KIIα variants. a, Kinase activity of PI4KIIα$^{SSPSS\Delta C}$ increases when Triton X-100 is replaced by a zwitterionic detergent, dimethyl(3-sulfopropyl) tetradecyl-ammonium hydroxide (Anzergent3-14, AZ3-14, Anatrace®) since the “negatively-charged head” of AZ3-14 can enhance electrostatic interactions between PI4KIIα and the surface of the detergent micelle. **b**, Comparison of the kinase activities of PI4KIIα variants measured at conditions PI/0.2% TX-100 and PI/0.1% AZ3-14. Error bars represent the standard deviation (s.d.) from three independent experiments.

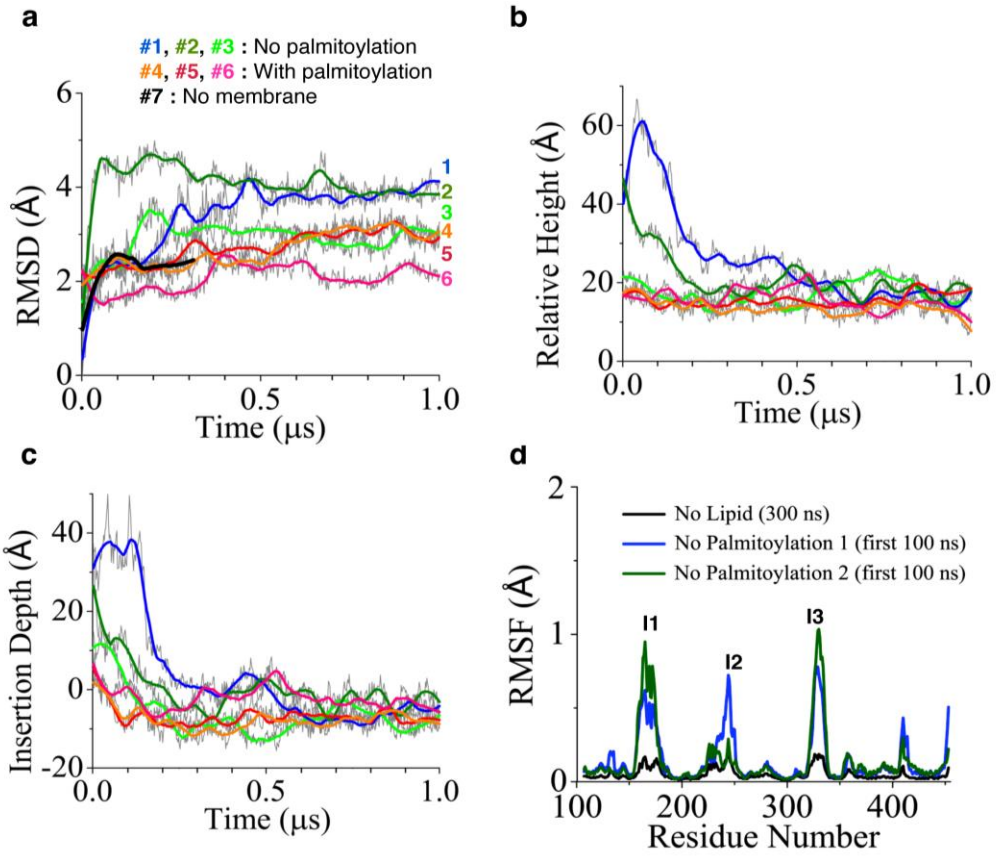

Supplementary Figure 7. Structural characterization of PI4KIIα in molecular dynamics simulations. a, Time evolution of RMSD of PI4KIIa relative to the crystal structure, with #1, #2 and #3 representing simulations of non-palmitoylated proteins, #4, #5 and #6 simulations of palmitoylated ones and #7 a simulation of membrane-free non-palmitoylated PI4KIIa. In simulations #1 and #2, the crystal structure of PI4KIIα was placed at t = 0 ns on top of the PI-containing membrane at a distance of 20 Å while in simulation #3 the distance was 10 Å. The average RMSD of non-palmitoylated and palmitoylated proteins relative to the crystal structure over the last 700 ns of 1-μs simulation were 3.59 Å and 2.64 Å, respectively. **b,** Time evolution of the relative height of the protein's center of mass with respect to upper lipid phosphate atoms' center of mass in different simulations. The choice of color is the same as in (**a**). **c,** Time evolution of the insertion depth of PI4KIIα's palmitoylation insertion (residue 166 to 179) center of

mass with respect to upper lipid phosphate atoms' center of mass. Negative values correspond to insertion of the loop into the membrane. The choice of color is the same as in (**a**). **d,** Conformational fluctuations of non-palmitoylated PI4KIIα in the absence of interactions with a membrane. The black curve represents the membrane-free simulation of PI4KIIα; blue and dark-green curves were obtained from the first 100 ns of non-palmitoylated PI4KIIα simulated in the presence of a membrane (#1 and #2 in a, b and c). The protein did not interact with the membrane during the first 100 ns of simulations #1 and #2., The RMSF was calculated using C_α-atoms of each protein residue (residue 107 to 453) through the indicated simulation time. For this purpose, the proteins were aligned to the crystal structure using backbone atoms without three insertions.

a

	Vmax （μmol/(L.min))	Km （mmol/L）
PI4KIIα^{FFPFF}	388.4±97.1	1.0±0.3
PI4KIIα^{CCPCC}	53.1±2.9	0.26±0.04
P-Value	0.004	0.01

b

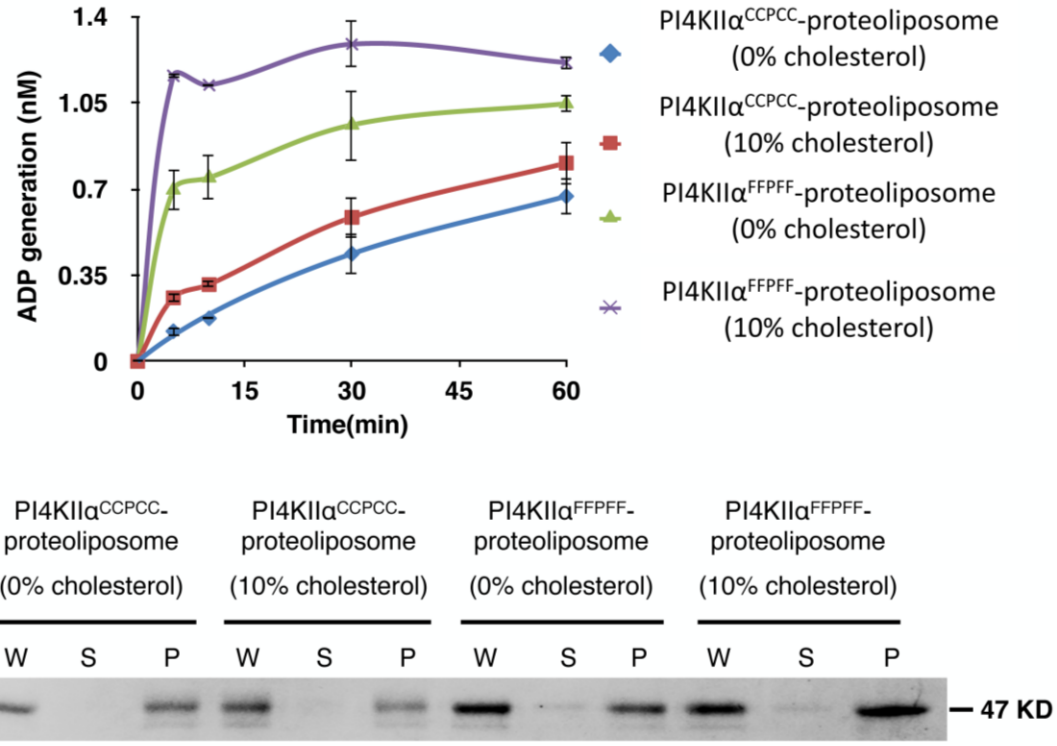

Supplementary Figure 8. Enzymatic assays of PI4KIIα variants. a. Enzymatic V_{max} and K_m of PI4KIIα variants. Lipid kinase activity of purified PI4KIIα^{FFPFF} and PI4KIIα^{CCPCC} (0.5 μg) was determined with the ADP-Glo^{TM} kinase kit (Promega). Effects of palmitoylation motif mutation on the kinetics of PI4KIIα catalysis were measured. V_{max} and K_m values for PI were calculated based on dose-dependent curves. Values are presented as means ± S.D. from three independent experiments (student's *t*-test). **b**, Lipid kinase activity of PI4KIIα variants on liposome with or without cholesterol. Proteoliposome of PI4KIIα variants were made according to **METHODS** with the lipid composition, 20% DOPE, 10% DOPS,

10% DOPA, 10% PI and 50% DOPC for the cholesterol-free system and 20% DOPE, 10% DOPS, 10% DOPA, 10% PI, 40% DOPC and 10% cholesterol for the cholesterol-containing system. The kinase reaction was initiated by adding 0.1 mM ATP and the kinase activity was plotted by monitoring ADP generation with the ADP-Glo^{TM} kinase kit (Promega). The error bars represent means ± S.D. from three independent experiments. The binding efficiencies of PI4KIIα variants to the liposome membrane were evaluated from the co-sedimentation experiments below. W: the whole amount of the proteoliposome; S, the supernatant after centrifuge of the proteoliposome; P, the precipitate after centrifuging the proteoliposome. Uncropped images of gels are shown in **Supplementary Fig. 9**.

Supplementary Figure 9

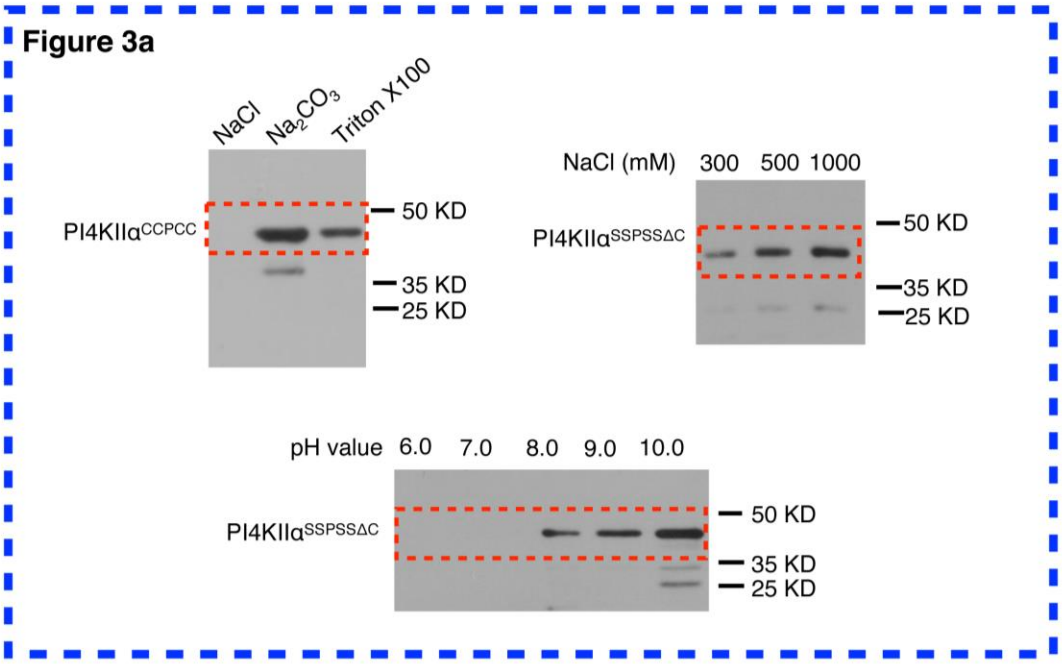

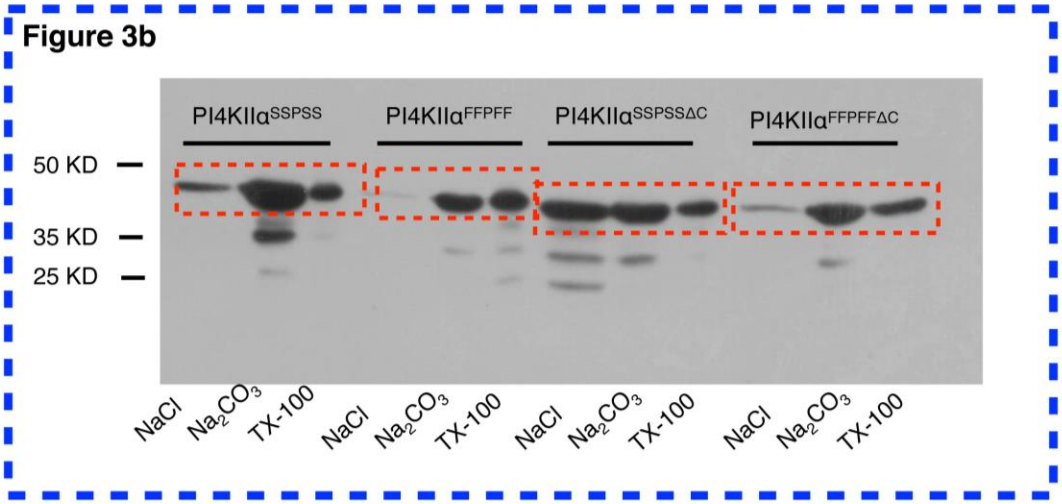

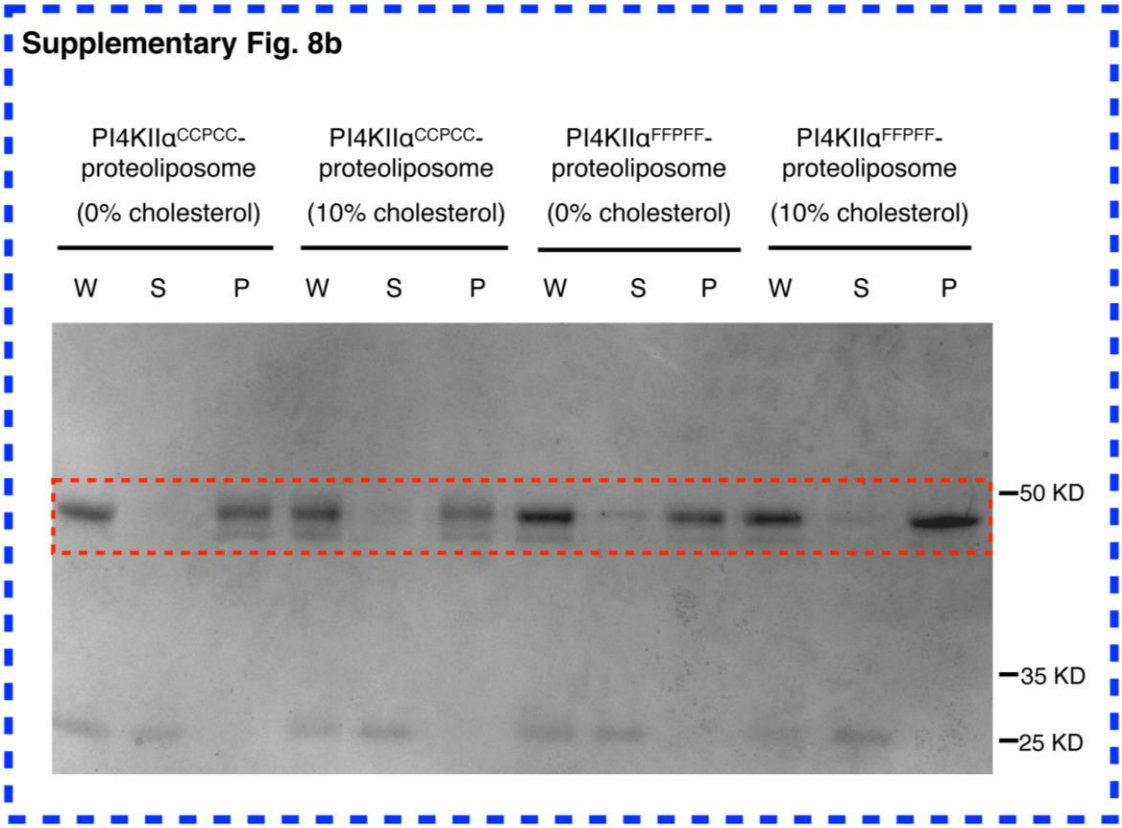

Supplementary Figure 9. Full scans of original Western blots and gels for data in Figure 3 and Supplementary Fig. 8. Panels corresponding to the figures in the paper are indicated.

Supplementary Table 1. Mutant constructs used in this study

Region	Name	Fragment	Mutation	Plasmids	Expression
Control	PI4KIIα$^{E\Delta N93}$	94-479	none	pFastBac	Insect cell (Hi5)
	PI4KIIα^{CCPCC}	78-479	none	pGEX-6P-1	*E. coli*
Palmitoylation motif and C terminal region (454-479)	PI4KIIα^{SSPSS}	78-479	^{174}SSPSS^{178}	pGEX-6P-1	*E. coli*
	PI4KIIα$^{SSPSS\Delta C}$	78-453	^{174}SSPSS^{178}	pGEX-6P-1	*E. coli*
	PI4KIIα^{FFPFF}	78-479	^{174} FFPFF^{178}	pGEX-6P-1	*E. coli*
	PI4KIIα$^{FFPFF\Delta C}$	78-453	^{174}FFPFF^{178}	pGEX-6P-1	*E. coli*
Nucleotide binding site	PI4KIIα$^{F263A/I345A}$	78-453	^{174}FFPFF^{178}/ F263A/I345A	pGEX-6P-1	*E. coli*
	PI4KIIα^{D269A}	78-453	^{174}FFPFF^{178}/ D269A	pGEX-6P-1	*E. coli*
	PI4KIIα^{K152A}	78-453	^{174}FFPFF^{178}/ K152A	pGEX-6P-1	*E. coli*
PI binding site	PI4KIIα$^{E157A/Y159A}$	78-479	E157A/Y159A	pGEX-6P-1	*E. coli*
	PI4KIIα$^{L184A/L349A}$	78-479	L184A/L349A	pGEX-6P-1	*E. coli*
Amphipathic α-helix of the palmitoylation insertion	PI4KIIα^{W166A}	78-479	W166A	pGEX-6P-1	*E. coli*
	PI4KIIα^{W169A}	78-479	W169A	pGEX-6P-1	*E. coli*
	PI4KIIα^{L170A}	78-479	L170A	pGEX-6P-1	*E. coli*
	PI4KIIα^{L173A}	78-479	L173A	pGEX-6P-1	*E. coli*
	PI4KIIα$^{W166A/W169A/L170A/L173A}$	78-479	W166A/W169A/ L170A/L173A	pGEX-6P-1	*E. coli*
	PI4KIIα$^{K165A/K168A/K172A}$	78-479	K165A/K168A/ K172A	pGEX-6P-1	*E. coli*
	PI4KIIα$^{K165E/K168E/K172E}$	78-479	K165E/K168E/ K172E	pGEX-6P-1	*E. coli*
Membrane binding sites	PI4KIIα^{W359A}	78-479	W359A	pGEX-6P-1	*E. coli*
	PI4KIIα^{Y365A}	78-479	Y365A	pGEX-6P-1	*E. coli*
	PI4KIIα^{W368A}	78-479	W368A	pGEX-6P-1	*E. coli*
	PI4KIIα$^{W359A/ Y365A/W368A}$	78-479	W359A/ Y365A/ W368A	pGEX-6P-1	*E. coli*
	PI4KIIα$^{R129A/R275A/R276A}$	78-479	R129A/R275A/ R276A	pGEX-6P-1	*E. coli*
	PI4KIIα$^{R129E/R275E/R276E}$	78-479	R129E/R275E/ R276E	pGEX-6P-1	*E. coli*
	PI4KIIα^{R129A}	78-479	R129A	pGEX-6P-1	*E. coli*

Supplementary Note 1

CHARMM36 force field [2-4] and the TIP3P water model [5] were used in all simulations. The simulations were carried out in an NPT ensemble; temperature was maintained at 310 K through a Langevin thermostat with a damping coefficient of 0.5 ps^{-1}; pressure was maintained at 1 atm with a Langevin-piston barostat [6]. Short-range non-bonded interactions were cut off smoothly between 1 and 1.2 nm; long-range electrostatics was computed with the PME algorithm [7]; simulations were performed with an integration time step of 2 fs in NAMD 2.9 [8].

For the force field of the palmitoylated cysteine residue, initial parameters were obtained from the amino acid cysteine and from the dioleoylphosphatidylcholine (DOPC) lipid tail, employing the corresponding CHARMM36 force field [4]. The full cysteine residue and the first three carbons of the palmitoylation group were selected for further optimization by the force field toolkit (FFTK) [9] plugin of VMD [10]. Partial atomic charges were optimized from water-interaction profiles by Gaussian [11] at a HF/6–31G(d) level of theory. Hydrogen atom charges were kept at 0.09e to be consistent with the CHARMM force field [12]. Bond and angle parameters were optimized from distortions along internal coordinates by means of a QM Hessian matrix calculation at a MP2/6–31G(d) level of theory. Dihedral terms using torsion scans were optimized at a MP2/6–31G(d) level of theory. Final parameters for palmitoylated cysteine residue are shown below.

Topology file:

```
ATOM   N    NH1      -0.47
ATOM   HN   H        0.31
ATOM   CA   CT1      0.07
ATOM   HA   HB1      0.09
GROUP                !     HA-CA--CB--SG
ATOM   1CB      CT2      -0.10
ATOM   HB1      HA2      0.09
ATOM   HB2      HA2      0.09
```

```
ATOM   1SG      SM       -0.08
GROUP
ATOM   C    C          0.51
ATOM   O    O          -0.51
GROUP              !        |     beta4
ATOM   C31      CL       0.67
ATOM   O32      OBL      -0.63
ATOM   C32      CTL2     -0.22
ATOM   H2X      HAL2     0.09
ATOM   H2Y      HAL2     0.09
GROUP
ATOM   C33      CTL2     -0.18
ATOM   H3X      HAL2     0.09
ATOM   H3Y      HAL2     0.09
GROUP
ATOM   C34      CTL2     -0.18
ATOM   H4X      HAL2     0.09
ATOM   H4Y      HAL2     0.09
GROUP
ATOM   C35      CTL2     -0.18
ATOM   H5X      HAL2     0.09
ATOM   H5Y      HAL2     0.09
GROUP
ATOM   C36      CTL2     -0.18
ATOM   H6X      HAL2     0.09
ATOM   H6Y      HAL2     0.09
GROUP
ATOM   C37      CTL2     -0.18
ATOM   H7X      HAL2     0.09
ATOM   H7Y      HAL2     0.09
GROUP
ATOM   C38      CTL2     -0.18
ATOM   H8X      HAL2     0.09
ATOM   H8Y      HAL2     0.09
GROUP
ATOM   C39      CTL2     -0.18
ATOM   H9X      HAL2     0.09
ATOM   H9Y      HAL2     0.09
GROUP
ATOM   C310     CTL2     -0.18
ATOM   H10X     HAL2     0.09
ATOM   H10Y     HAL2     0.09
```

```
GROUP
ATOM   C311    CTL2    -0.18
ATOM   H11X    HAL2    0.09
ATOM   H11Y    HAL2    0.09
GROUP
ATOM   C312    CTL2    -0.18
ATOM   H12X    HAL2    0.09
ATOM   H12Y    HAL2    0.09
GROUP
ATOM   C313    CTL2    -0.18
ATOM   H13X    HAL2    0.09
ATOM   H13Y    HAL2    0.09
GROUP
ATOM   C314    CTL2    -0.18
ATOM   H14X    HAL2    0.09
ATOM   H14Y    HAL2    0.09
GROUP
ATOM   C315    CTL2    -0.18
ATOM   H15X    HAL2    0.09
ATOM   H15Y    HAL2    0.09
GROUP
ATOM   C316    CTL3    -0.27
ATOM   H16X    HAL3    0.09
ATOM   H16Y    HAL3    0.09
ATOM   H16Z    HAL3    0.09
```

Parameter file:

```
BONDS

SM   CL   188.316      1.800

ANGLES

CT2   SM   CL      93.502     105.512
SM    CL   OBL     44.869     117.121
SM    CL   CTL2    48.393     120.173

CT1   CT2   SM      CL      1.0040     3   180.00
CT2   SM    CL      OBL     2.7020     1   0.00
CT2   SM    CL      OBL     2.6500     2   180.00
CT2   SM    CL      CTL2    2.4760     1   180.00
```

CT2	SM	CL	CTL2	2.2270	2	180.00
SM	CL	CTL2	HAL2	0.2320	3	0.00
HA2	CT2	SM	CL	0.7170	3	0.00

Supplementary References

1. Pettersen, E.F. et al. UCSF Chimera--a visualization system for exploratory research and analysis. *J Comput Chem* **25**, 1605-12 (2004).
2. Schlenkrich, M., Brickmann, J., MacKerell Jr, A.D. & Karplus, M. An empirical potential energy function for phospholipids: criteria for parameter optimization and applications. in *Biological Membranes* 31-81 (Springer, 1996).
3. MacKerell, A.D. et al. All-atom empirical potential for molecular modeling and dynamics studies of proteins. *The Journal of Physical Chemistry B* **102**, 3586-3616 (1998).
4. Klauda, J.B. et al. Update of the CHARMM all-atom additive force field for lipids: validation on six lipid types. *The Journal of Physical Chemistry B* **114**, 7830-7843 (2010).
5. Jorgensen, W.L., Chandrasekhar, J., Madura, J.D., Impey, R.W. & Klein, M.L. Comparison of simple potential functions for simulating liquid water. *The Journal of Chemical Physics* **79**, 926-935 (1983).
6. Martyna, G.J., Tobias, D.J. & Klein, M.L. Constant pressure molecular dynamics algorithms. *The Journal of Chemical Physics* **101**, 4177 (1994).
7. Darden, T., Toukmaji, A. & Pedersen, L. Long-range electrostatic effects in biomolecular simulations. *Journal de chimie physique* **94**, 1346-1364 (1997).
8. Phillips, J.C. et al. Scalable molecular dynamics with NAMD. *Journal of Computational Chemistry* **26**, 1781-1802 (2005).
9. Mayne, C.G., Saam, J., Schulten, K., Tajkhorshid, E. & Gumbart, J.C. Rapid parameterization of small molecules using the Force Field Toolkit. *J Comput Chem* **34**, 2757-70 (2013).
10. Humphrey, W., Dalke, A. & Schulten, K. VMD: Visual molecular dynamics. *Journal of Molecular Graphics* **14**, 33-38 (1996).
11. Frisch, M. et al. Gaussian 09, revision A. 02; Gaussian. *Inc., Wallingford, CT* **270**, 271 (2009).
12. Yin, D. & MacKerell, A.D. Combined ab initio/empirical approach for optimization of Lennard–Jones parameters. *Journal of Computational Chemistry* **19**, 334-348 (1998).